Air-Stable Near-Infrared $AgInSe_2$ Nanocrystals

Marc-Antoine Langevin,[†,‡] Anna M. Ritcey,[†,‡] and Claudine Nì Allen[†,*]

[†]Centre d'Optique, Photonique et Laser (COPL), Département de Physique, de Génie Physique et d'Optique, Université Laval, 2375 Rue de la Terrasse, Québec, QC, Canada G1V 0A6 and [‡]Centre de Recherche sur les Matériaux Avancés, Département de Chimie, Université Laval, 1045 Avenue de la Médecine, Québec, QC, Canada G1V 0A6

ABSTRACT We present the synthesis of air-stable $AgInSe_2$ nanocrystals *via* thermolysis of an Ag—In—thiolate complex followed by an anion exchange reaction. Evolution of the Ag:In:Se ratio with the reaction time demonstrates progressive incorporation of In^{3+} in β-Ag_2Se seeds. While their lattice stays in the metastable orthorhombic crystal structure, the final $AgInSe_2$ nanocrystal shape can be spherical, pyramidal, or prismatic depending on reaction conditions. These nanocrystals emit from trap states between 800 and 1300 nm, which is a biologically and technologically important near-infrared range, with a photoluminescence quantum yield up to an order of magnitude of 21%. The appearance of a shoulder within the photoluminescence spectra between 845 and 890 nm is correlated to the presence of prismatic nanocrystals.

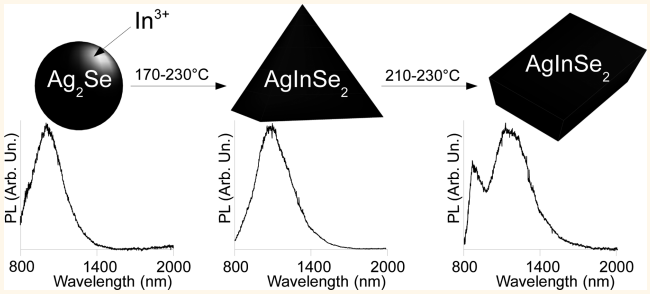

KEYWORDS: nanocrystal synthesis · near-infrared photoluminescence · silver indium selenide · anion exchange · air-stable quantum dots · shape-dependent optical properties

The near-infrared (NIR) optical region is interesting for many applications such as biological imaging, solar cells, and telecommunications.[1−4] Inorganic semiconductor nanocrystals (NCs) are promising materials for these applications because of their tunable absorption and emission properties. They are considered to be more chemically robust and photostable than organic fluorophores and they typically offer a higher photoluminescence (PL) quantum yield (Φ_F). They can also be functionalized with different ligands to target specific organs or diseases.

Only a few compounds with the narrow bandgap (<~1.5 eV) needed to reach this wavelength range have been synthesized as colloidal NCs. Most NCs exhibiting efficient absorption and emission in this optical region are based on toxic elements, such as cadmium, arsenic, mercury, and lead.[5−12] Even if small Cd and Pb-based NCs have shown favorable renal clearance, many unwanted side effects have been associated with the use of these materials.[13] More recently, NCs based on less toxic elements, such as silver, copper and/or indium have been developed.[14−19] Among these, some I (Ag, Cu)—III (In, Ga)—VI (S, Se, Te)$_2$ compounds show tunable absorption and emission wavelengths with reasonable Φ_F values and, furthermore, demonstrate potential for nonlinear optical properties. These I—III—VI$_2$ semiconductors are especially promising NC materials because of their ability to form different alloys enabling a modulation of their properties.[20] For example, the Φ_F of I—III—VI$_2$ NCs can be modified through the I:III ratio or by inserting Zn in the alloy.[21,22] NCs can also be covered with shells to protect the cores and increase their Φ_F.[16] However, before tuning these alloys, it is relevant to synthesize stoichiometric I—III—VI$_2$ NCs that emit radiatively in the NIR, as done for $CuInS_2$, $CuInSe_2$, $CuInTe_2$, and $AgInS_2$.

Since 2006, a few syntheses of $AgInSe_2$ NCs have been reported, but the possibility of photoexcitation and radiative emission was demonstrated only for those prepared by Bawendi's group.[23−27] However, the small size of their NCs resulted in visible photoluminescence from orange to red. Further issues with these NCs were their nonstoichiometry, the presence of an important amount of Ag^0 and the use of highly volatile and

* Address correspondence to claudine.allen@phy.ulaval.ca.

Received for review December 16, 2013 and accepted March 17, 2014.

Published online March 17, 2014
10.1021/nn406439w

hazardous bis(trimethylsilyl)selenide in the synthetic method. The synthesis of stoichiometric ternary NCs can be difficult due to the necessity of balancing the reactivity of the precursors, but can be done *via* thermolysis with less hazardous precursors.[28]

In this article, we present a synthetic method based on the thermolysis of an Ag−In−thiolate complex followed by an anion exchange reaction to obtain $AgInSe_2$ colloidal NCs emitting in the NIR. The transmission electron microscopy (TEM) images revealed the presence of spherical [I], pyramidal [II], and prismatic [III] NCs, depending on reaction conditions. Energy dispersive X-ray spectroscopy (EDS) shows the progressive incorporation of In^{3+} in the NCs whereas powder X-ray diffractograms (XRD) exhibit peaks characteristic of an orthorhombic phase. We propose a reaction mechanism taking into consideration these observations. Absorption and photoluminescence spectroscopies were used to monitor the reactions at different temperatures, which revealed a correlation between NC shape and optical properties.

RESULTS AND DISCUSSION

$AgInSe_2$ NC Synthesis. Following the synthetic method presented by Zhong *et al.* for stoichiometric $CuInSe_2$ NCs, we prepared an Ag−In−thiolate complex by mixing silver oxide, indium acetate, and dodecanethiol in octadecene.[17] The complex is then thermodegraded at high temperature in the presence of oleylamine as a second ligand. A solution containing TBP−Se is quickly injected, initiating an anion exchange reaction resulting in the formation of $AgInSe_2$ NCs. This exchange occurs because P−S bonds (403 kJ/mol) are stronger than P−Se bonds (315 kJ/mol).[29] Oleylamine offers a better dispersibility of the NCs than does oleic acid previously used by Zhong *et al.*[17] Surprisingly, when silver acetate, silver chloride, or silver iodide are used as silver sources, a black precipitate is formed immediately after the injection of the TBP−Se solution. In our synthetic conditions, no reaction is observed below 150 °C and precipitation of the product occurs above 250 °C, so the effects of reaction time were studied at temperatures of 170, 190, 210, and 230 °C.

Physical and Morphological Properties of $AgInSe_2$ NCs. Elemental analysis was performed on NC aliquots sampled at different reaction times after the injection of TBP-Se. The evolution of the Ag:In:Se ratio, as measured by EDS, is reported in Table 1 and indicates a composition close to Ag_2Se at shorter reaction times, followed by a gradual incorporation of In^{3+} to finally reach near-stoichiometric $AgInSe_2$ NCs. We observe a slight deviation from stoichiometry, with indium reaching about 30% instead of 25% of the total composition of mature NCs. The shortest reaction time for each temperature corresponds to the first light-emitting aliquots, which are mostly Ag_2Se NCs containing 8−10% of indium. Measurement of the sulfur content in the core was also attempted. However, since we used dodecanethiol as a ligand, it is the main contribution to the relative sulfur content detected; it is not representative of sulfur anions in the core.

TABLE 1. Atomic Percentages of Ag, In, and Se Measured by EDS for $AgInSe_2$ NCs Prepared at Different Reaction Temperatures and Times[a]

temperature (°C)	reaction time (min)	%Ag	%In	%Se
170	90	58 ± 2	7.9 ± 0.3	34 ± 1
	150	30.7 ± 0.3	24.5 ± 0.6	44.8 ± 0.5
	300	29 ± 1	26.1 ± 0.7	45 ± 1
190	15	55 ± 6	11 ± 6	33 ± 1
	150	29 ± 1	27.5 ± 0.8	44 ± 2
	300	26.0 ± 0.6	30.5 ± 0.4	43.6 ± 0.5
210	5	51 ± 4	10 ± 2	38 ± 2
	60	30.4 ± 0.3	27.3 ± 0.4	42.3 ± 0.5
	150	27.6 ± 0.7	32 ± 1	41 ± 1
	300	27.3 ± 0.4	30.7 ± 0.6	41.8 ± 0.8
230	3	54 ± 2	11 ± 2	35 ± 1
	90	27.4 ± 0.6	30 ± 1	41 ± 2
	180	27 ± 1	30 ± 1	44 ± 2

[a] Results indicate the progressive incorporation of In^{3+} in the Ag_2Se NCs, leading to the formation of near-stoichiometric $AgInSe_2$ NCs.

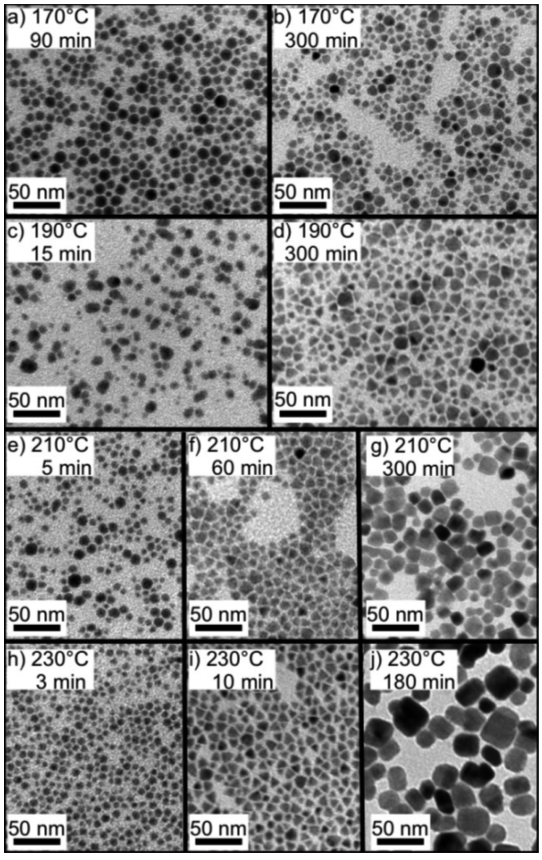

Figure 1. TEM images of $AgInSe_2$ NCs synthesized between 170 and 230 °C for aliquots taken at different reaction times indicated in the left corner. Images show the presence of spherical [I] (a, c, e, and h), pyramidal [II] (b, d, f, and i), and prismatic [III] (g and j) NCs.

TEM images corresponding to the various aliquots are shown in Figure 1. Three different NC shapes are

observed. At all reaction temperatures, the first light-emitting NCs are initially primarily spherical [I] and are polydisperse in size. However, once the reaction is complete, the mature NCs are either pyramidal [II], when synthesized at 170 and 190 °C (Figure 1b,d), or prismatic [III] when synthesized at 210 and 230 °C (Figure 1g,j). Figure 1f,l also shows the formation of pyramidal NCs grown at 210 °C after 1 h and at 230 °C after 10 min, prior to reaching maturity, indicating that the prismatic shape comes from the ripening of the pyramidal NCs. Image analysis shows no significant effect of the temperature on the size of pyramidal NCs. We measured essentially the same average diameter of (10 ± 2) nm for pyramid-shaped NCs prepared at 190 °C after 5 h, 210 °C after 1 h, and 230 °C after 10 min and (9 ± 2) nm for NCs synthesized at 170 °C after 5 h. However, prism-shaped NCs [III] synthesized at 210 °C after 5 h have an average diameter of (16 ± 3) nm and those synthesized at 230 °C after 3 h have an average diameter of (23 ± 6) nm.

I–III–VI_2 materials exist mostly in two different crystal phases: the thermodynamically stable tetragonal phase and the metastable orthorhombic phase.[26] Here, the diffractograms obtained for all the NCs did not correspond to the tetragonal phase of $AgInSe_2$ because of the extra peaks at 24, 27, 36, and 47°.[30] Instead, they resemble orthorhombic $AgInS_2$ diffractograms shifted toward smaller angles by about 2°, including a small shoulder for the 43° peak distinguishing between hexagonal and orthorhombic phases.[27,30] This shift is expected since the $AgInSe_2$ unit cell is larger than the $AgInS_2$ unit cell. Furthermore, our diffractograms match those acquired by Vittal's group, which they attributed to orthorhombic $AgInSe_2$ NCs, as indicated by dashed lines in Figure 2.[23] We also observed sight variations in the relative intensity of the peaks depending either on sample preparation for XRD analysis or on the reaction conditions. The diffractogram obtained for the NCs grown at 170 °C is also slightly shifted toward smaller angles compared to the others, probably due to the smaller content in indium, as seen in Table 1. To the best of our knowledge, tetragonal $AgInSe_2$ NCs were only observed by Abazović *et al.* so far, when they used a phosphine and myristic acid as ligands.[26] With our synthetic method, when we replaced oleylamine with myristic acid at 190 °C, we still obtained orthorhombic $AgInSe_2$ NCs and also an important amount of Ag^0.

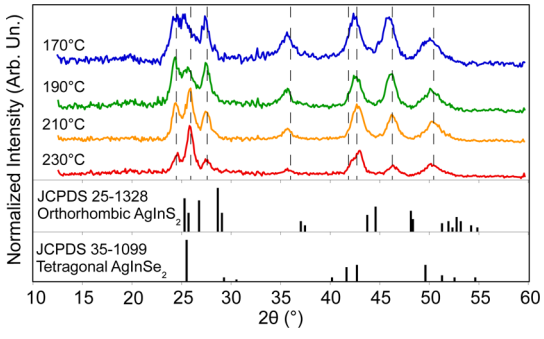

Figure 2. XRD patterns of NCs synthesized at 170, 190, and 210 °C after 5 h and at 230 °C after 3 h. The dashed lines correspond to the positions of the peaks observed by Vittal's group for orthorhombic $AgInSe_2$.

Reaction Mechanism. Ogawa *et al.* proposed a mechanism for the synthesis of $AgInS_2$ NCs that could explain the presence of the orthorhombic phase.[31] An adaptation of this reaction mechanism could also explain our observations of gradual incorporation of indium in the NCs as well as their different shapes. First, the reaction of silver and indium precursors with DDT forms an Ag–In–thiolate complex. When it is thermolyzed with an amine in the mixture, monoclinic Ag_2S seeds and $(R\text{-}NH)_3In$ complex are likely obtained. Indeed, by increasing the reaction temperature, the solution color changes from light yellow to brown, indicating the formation of Ag_2S seeds. When the solution is cooled before injecting the Se precursor, it gives a gray-brown precipitate. XRD analysis of this precipitate does not show if it contains Ag_2S, as these seeds were likely too small or too amorphous (Supporting Information Figure S1). Proceeding with the regular protocol, XRD analysis, performed up to 1 min after injecting the TBP–Se solution, shows the formation of orthorhombic (β) Ag_2Se NCs and progressive consumption of the In complex (see Supporting Information Figure S1). Since the Ag:Se ratio evolves from 2:1 to 1:2 as presented in Table 1, the ripening process should also involve incorporation of Se to reach near-stoichiometric $AgInSe_2$ NCs. Scheme 1 presents a graphical summary of the proposed mechanism including the evolution of the NCs' shape from spheres [I] to pyramids [II] to prisms [III], as observed by TEM.

The thermolysis of an Ag–In–thiolate complex without addition of a second ligand was shown to generate Ag^0 cores surrounded by $AgInS_2$ wires.[31] According to Zhong *et al.*, thermolysis of Cu–In–thiolate directly leads to the formation of ternary $CuInS_2$ seeds. Without the addition of a second ligand, $CuInS_2$ seeds would tend to grow by oriented attachment, forming nanorods.[28] Although a similar reaction mechanism might be expected with a single different element in the

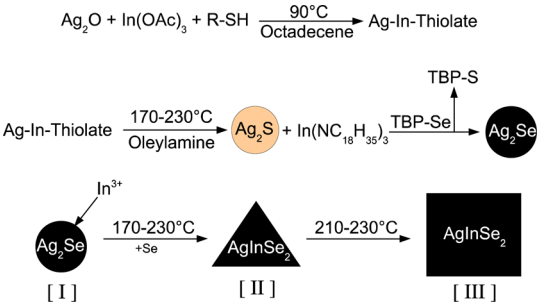

Scheme 1. Proposed mechanism for the formation of $AgInSe_2$ NCs.

precursor, the divergence in thermolysis products justifies our proposition of initial nucleation of In-free Ag_2S seeds in the presence of a second ligand, in agreement with the mechanism from Ogawa *et al.* for the formation of $AgInS_2$ NCs.[31]

Optical Properties of $AgInSe_2$ NCs. Figure 3a presents normalized PL spectra for spherical Ag_2Se NCs containing 10% of indium [I] as well as transitory pyramidal [II] and mature prismatic [III] $AgInSe_2$ NCs synthesized at 210 °C. The spectra for [I] and [II] consist of only one large PL peak, while a smaller shoulder at shorter wavelengths appears for prism-shaped NCs [III]. The width of the peaks could partially be attributed to the NC size polydispersity. However, it is already well-known for I−III−VI_2 materials that PL emission mostly comes from transitions between states of donor−acceptor pairs induced by defects in the NCs such as chalcogenide vacancies, silver vacancies, chalcogenide interstitials, silver interstitials, *etc.*[19,32−34] Many of these trap states, distributed in energy, can be populated through thermalisation after photoexcitation and then they relax radiatively, so the resulting PL peak is always broader than 100 nm. Transitions are expected to exhibit a large Stokes shift relative to the NC absorption band. Indeed, spectra in Figure 3b show almost no absorption at wavelengths longer than 900 nm, despite a PL emission occurring after 1000 nm.

Figure 4a shows the central wavelength of the broad peak varying between 955 and 1250 nm as a function of reaction time. Redshifts of this peak can be associated with the three steps in the reaction mechanism. First, we observe redshifts of more than 70 nm in the first minutes after the appearance of the photoluminescent NCs. This likely comes from a progressive incorporation of In^{3+} in the β-Ag_2Se NC seeds [I]. Then, we observe a plateau around (1080 ± 10) nm, which could be associated with emission spectra

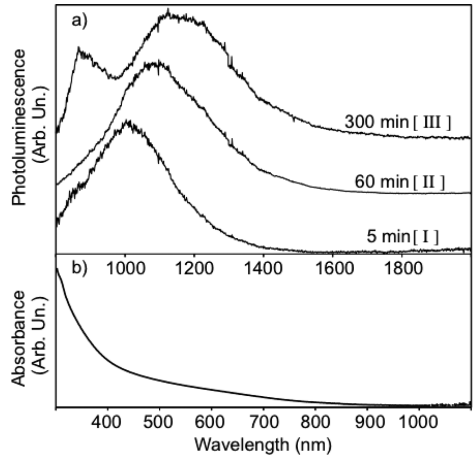

Figure 3. (a) PL spectra of NCs synthesized at 210 °C after 5, 60, and 300 min. Roman numerals correspond to the shape of the NCs presented in Scheme 1: [I] sphere, [II] pyramid, and [III] prism. (b) Absorption spectrum obtained for $AgInSe_2$ NCs synthesized at 210 °C after 300 min.

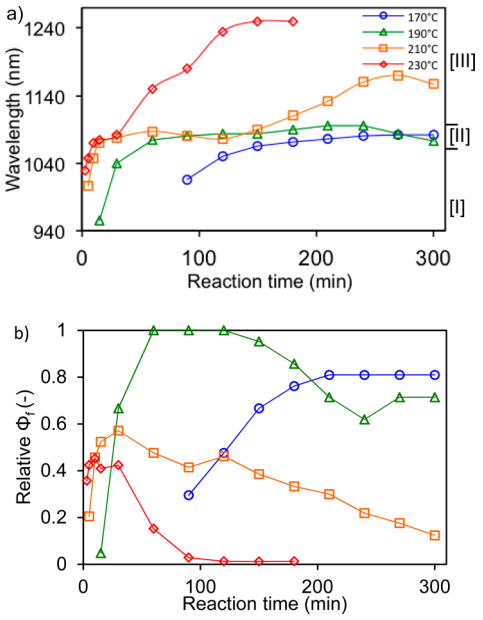

Figure 4. (a) Central wavelength of the broader PL emission peak as a function of the reaction time. The plateaus around 1080 nm correspond to the emission from traps in pyramid-shaped NCs [II], resuming redshifting and growing into prisms [III] at higher temperatures. (b) Quantum yield, relative to the maximum value of 21%, as a function of the reaction time. Results are presented for NCs synthesized at 170 °C (blue circles), 190 °C (green triangles), 210 °C (orange squares), and 230 °C (red diamonds). The colored lines are a guide to the eye.

characteristic of defects in pyramidal near-stoichiometric $AgInSe_2$ NCs [II]. At 170 and 190 °C, this phase seems to be stable, at least for the first 5 h of reaction. However, this step is only transitory for reaction temperatures of 210 and 230 °C and is shorter for higher temperature. Indeed, the redshift resumed after 150 min and almost immediately at 210 and 230 °C, respectively. This likely coincides with a shape transition from pyramidal [II] to prismatic [III] NCs and their ripening since the mature NCs presented in Figure 2g,l are prismatic and bigger.

Since pyramidal NCs [II] all reach similar sizes and emission spectra, we cannot conclude if the defects and their radiative transitions are affected by changes in pyramidal NC size. However, the prismatic NCs [III] continued growth and spectral redshift suggest that the energy distribution of radiative trap states was modified by the increasing NC size in this case, coinciding with the appearance of radiative transitions from a second set of trap states at higher energies. Indeed, radiative transitions from these states appear in the spectra after 120 min of reaction at 210 °C and 30 min at 230 °C, corresponding to the change in morphology from [II] to [III] and ripening of the prism-shaped NCs as well as progressive loss of their PL intensity (Figure 4b).

The presence of multiple PL peaks was already observed in $CuInS_2$ and $AgInS_2$.[22,35] According to Mao

et al., the main large peak observed for $AgInS_2$ would be radiative emission from intrinsic trap states, while the more energetic and narrower one would come from surface defects. Whereas their relative PL intensity of higher to lower energy peaks decreases with the surface/volume ratio as the NCs grow, ours follow the opposite trend (see Supporting Information Figure S2). Our results instead suggest a correlation with the NC shape: although PL spectra of [I] and [II] may potentially contain some weaker and convolved version of this narrow peak at high energy, it is only observed for prismatic NCs. It is possible the nature of radiative defects of pyramidal [II] and prismatic [III] NCs might not be the same, especially if they are located on different NC facets. In contrast to the behavior of $AgInS_2$ NCs, we observed fluctuations in the spectral position of the higher energy peak between 845 and 890 nm, but there is no systematic correlation with the reaction time. To the best of our knowledge, correlation between relative intensity of PL peaks and shape of I−III−VI_2 NCs has not been previously shown, and further investigations on the defects of I−III−VI_2 NCs will be needed to better understand their nature and their impact on photophysical properties in different surroundings.[36]

We measured a (Φ_F) as high as an order of magnitude of 21% for NCs synthesized at 190 °C with a reaction time between 60 and 150 min, used as normalization reference in Figure 4b. Since Cu-based I−III−VI_2 NCs are known to quickly lose their PL when exposed to air, it was also relevant to characterize the stability of this emission.[16] We used purified pyramid-shaped $AgInSe_2$ NCs prepared with a 5-h synthetic reaction at 190 °C for the air-stability test. One day after the synthesis, we measured a Φ_F of 13% and a PL wavelength centered at (1073 ± 5) nm that remained stable for at least one week. After a month, we observed a slight blue shift of 20 nm and measured a Φ_F of 15%. This could be attributed to the precipitation of larger and possibly slightly prismatic NCs, since size-selective precipitation is known to affect PL spectrum of I−III−VI_2 NCs.[37] Therefore, we conclude that our NCs are already reasonably stable for at least one month at ambient conditions without addition of any shell.

CONCLUSION

In conclusion, we synthesized, *via* thermolysis followed by an anion-exchange reaction, $AgInSe_2$ NCs with a Φ_F as high as an order of magnitude of 21% emitting between 800 and 1300 nm. The reaction mechanism most likely implied gradual incorporation of In^{3+} in spherical β-Ag_2Se NCs, thus only allowing the formation of the metastable orthorhombic phase of $AgInSe_2$. These NCs became pyramid-shaped and, depending on the reaction temperature, eventually ripened into larger prism-shaped NCs, which was linked to the appearance of a shoulder on the higher energy side of the PL spectra.

EXPERIMENTAL SECTION

Chemicals. The following chemicals were used: silver(I) oxide (Ag_2O, 99+% metal basis, Alfa Aesar); indium(III) acetate ($In(OAc)_3$, anhydrous 99.99% trace metal basis, Acros Organics); 1-dodecanethiol (DDT, 98%, Alfa Aesar); 1-octadecene (ODE, technical grade 90%, Alfa Aesar); oleylamine (OLA, technical grade 70%, Sigma Aldrich); selenium powder (Se, ~100 mesh ≥99.5% trace metal basis, Sigma Aldrich); tributylphosphine (TBP, 97%, Sigma Aldrich); tetrachloroethylene (TCE, technical grade, Anachemia); acetone (certified ACS, Fisher Scientific); indocyanine green (ICG, Cardiogreen, Sigma Aldrich).

Synthesis of $AgInSe_2$ NCs. $AgInSe_2$ NCs were synthesized using 0.025 mmol (5.8 mg) of Ag_2O, 0.05 mmol (14.6 mg) of $In(OAc)_3$, and 0.25 mL of DDT dissolved in 5 mL of ODE. The solution was degassed under vacuum for 30 min at 90 °C to form the Ag−In−thiolate complex and 0.25 mL of OLA was injected in the reaction flask. The solution was degassed for and additional 30 min under vacuum and was then put under N_2 atmosphere using a standard Schlenk-line technique. The solution was heated to 170, 190, 210, or 230 °C and 0.2 mL of Se precursor was quickly injected. This Se precursor was prepared by dissolving 1 mmol (79 mg) of Se in 0.25 mL of TBP and 0.75 mL of ODE. After precursor injection, the suspension was allowed to react for 5 h at constant temperature, except for the reaction at 230 °C that was stopped after 3 h to avoid precipitation of the sample. Subsequently, 0.1 mL aliquots were taken after 1, 3, 5, 10, 15, 30 min and then every 30 min until the end of the reaction. The aliquots were dispersed in 1 mL of TCE for the different analyses. The suspension was purified by centrifugation in acetone and dispersed in 3 mL of TCE.

UV−Visible Measurements. Absorption spectra of the samples and the reference fluorophore were recorded at room temperature with a Varian Cary 50 Conc UV−visible spectrophometer from 300 to 1100 nm. The absorbance at 488 nm was kept between 0.05 and 0.1 to have enough PL intensity in subsequent measurements while avoiding autoabsorption from the NCs.

Photoluminescence Measurements. PL spectra were recorded between 800 and 2000 nm with a Jobin Yvon Nanolog equipped with a Symphony-II CCD detector. Indocyanine Green (ICG) dissolved in dimethyl sulfoxide (DMSO) was used as a reference fluorophore (Φ_F = 0.13).[16] The excitation wavelength was set to 488 nm for $AgInSe_2$ NCs and 795 nm for ICG. The excitation and emission slits were set at 10-nm resolution and a 540-nm high-pass filter was used to cut the second harmonic of the excitation. Each spectrum was obtained by adding 10 scans of 5 s. PL was corrected by the lamp intensity at each wavelength to allow a comparison between the NCs and the reference fluorophore. The PL peaks position was determined by fitting one or two log-normal distribution on the spectra with a spectrum treatment software (Fityk).

Energy Dispersive X-ray Spectroscopy. EDS measurements were obtained with a Quanta 3D FEG scanning electron microscope from the FEI Company using an EDAX Si(Li) detecting unit. NC samples were centrifuged with acetone two additional times to remove as much ligands and impurities as possible and were dispersed in chloroform. Drops of each suspension were then put on an aluminum surface and scanned with a 10 kV electron beam to separate sufficiently the Ag Lα and In Lα lines.

Powder X-ray Diffraction. Diffractograms were acquired using a Siemens/Bruker X-ray diffractometer with a 2D Hi-Star XRD detector. The radiation source was a Kristalloflex 760 with a nickel window emitting the Cu Kα line (λ = 1.5418 Å) with an accelerating voltage and current of 40 kV and 40 mA,

respectively. Purified NC suspensions were again centrifuged twice with acetone to remove as much ligands as possible prior to the analysis. Diffractograms were recorded from 10 to 60°. The background signal was automatically subtracted by the diffraction pattern treatment software GADDS.

Transmission Electron Microscopy. The NCs were imaged with a JEOL JEM 1230. For each sample, 200 NCs were measured by fitting circles around NCs and extracting their diameter using an image treatment software (ImageJ).

Fluorescence Quantum Yield. Φ_F was determined as presented by Williams *et al.*[38] First, UV−visible absorption spectra were acquired for the ICG reference at different concentrations. Measurements were taken at low concentrations in order to avoid reabsorption that would result in nonlinear effects affecting the calculated Φ_F values. PL spectra were then recorded for each dilution and the data of integrated PL intensity (in photons) *vs* absorbance at λ_{abs} = 795 nm for ICG and λ_{abs} = 488 nm for $AgInSe_2$ NCs was plotted. The same procedure was followed for every NC sample. Φ_F was calculated with eq 1:

$$\Phi_F = \Phi_{ICG}\left(\frac{Grad_{NCs}}{Grad_{ICG}}\right)\left(\frac{\eta^2_{TCE}}{\eta^2_{DMSO}}\right) \quad (1)$$

where Grad is the gradient of the data plotted and η is the refractive index of the solvent. In the case of aliquot, absorption and emission spectra were acquired for one concentration that was below absorption saturation at λ_{abs} = 488 nm. Their integrated emission intensity was then compared to the value obtained for the associated final NC sample to calculate the relative Φ_F.

Conflict of Interest: The authors declare no competing financial interest.

Supporting Information Available: XRD patterns for $AgInSe_2$ precursors; absorption and photoluminescence spectrum of aliquots obtained after different reaction times at different temperatures. This material is available free of charge *via* the Internet at http://pubs.acs.org.

Acknowledgment. The authors thank Patrick Larochelle, Stéphan Gagnon, Rodica N. Plesu, and Wenhua Bi for their technical support. This work was supported by the Natural Sciences and Engineering Research Council of Canada (NSERC) and Fonds de Recherche du Québec-Nature et Technologies (FRQ- NT).

REFERENCES AND NOTES

1. Michalet, X.; Pinaud, F. F.; Bentolila, L.; Tsay, J. M.; Doose, S.; Li, J. J.; Sundaresan, G.; Wu, M.; Gambhir, S. S.; Weiss, S. Quantum Dots for Live Cells, *in Vivo* Imaging, and Diagnostics. *Science* **2005**, *307*, 538–544.
2. Medintz, I. L.; Uyeda, H. T.; Goldman, E. R.; Mattoussi, H. Quantum Dot Bioconjugates for Imaging, Labelling and Sensing. *Nat. Mater.* **2005**, *4*, 435–446.
3. Ramsamy, K.; Nejo, A. O.; Ziqubu, N.; Rajasekhar, P. V. S. R.; Nejo, A. A.; Revaprasadu, N.; O'Brien, P. A New Route To Lead Chalcogenide Nanocrystals. *J. Inorg. Chem. Soc.* **2011**, *133*, 17598–17601.
4. Ainslie, B. J.; Craig, S. P.; Davey, S. T. The Absorption and Fluorescence Spectra of Rare Earth Ions in Silica-Based Monomode Fiber. *J. Lightwave Technol.* **1988**, *6*, 287–293.
5. Kim, S.; Lim, Y. T.; Soltesz, E. G.; De Grand, A. M.; Lee, J.; Nakayama, A.; Parker, J. A.; Mihaljevic, T.; Laurence, R. G.; Dor, D. M.; *et al.* Near-Infrared Fluorescent Type II Quantum Dots for Sentinel Lymph Node Mapping. *Nat. Biotechnol.* **2004**, *22*, 93–97.
6. Harris, D. K.; Allen, P. M.; Han, H.-S.; Walker, B. J.; Lee, J.; Bawendi, M. G. Synthesis of Cadmium Arsenide Quantum Dots Luminescent in the Infrared. *J. Am. Chem. Soc.* **2011**, *133*, 4676–4679.
7. Higginson, K. A.; Kuno, M.; Bonevich, J.; Qadri, S. B.; Yousuf, M.; Mattoussi, H. Synthesis and Characterization of Colloidal β-HgS Quantum Dots. *J. Phys. Chem. B* **2002**, *106*, 9982–9985.
8. Keuleyan, S.; Lhuillier, E.; Guyot-Sionnest, P. Synthesis of Colloidal HgTe Quantum Dots for Narrow Mid-IR Emission and Detection. *J. Am. Chem. Soc.* **2011**, *133*, 16422–16424.
9. Lifshitz, E.; Brumer, M.; Kigel, A.; Sashchiuk, A.; Bashouti, M.; Sirota, M.; Galun, E.; Burshtein, Z.; Le Quang, A. Q.; Ledoux-Rak, I.; *et al.* Air-Stable PbSe/PbS and PbSe/$PbSe_xS_{1-x}$ Core-Shell Nanocrystal Quantum Dots and Their Applications. *J. Phys. Chem. B* **2006**, *110*, 25356–25365.
10. Moreels, I.; Lambert, K.; De Muynck, D.; Vanhaecke, F.; Poelman, D.; Martins, J. C.; Allan, G.; Hens, Z. Composition and Size-Dependent Extinction Coefficient of Colloidal PbSe Quantum Dots. *Chem. Mater.* **2007**, *19*, 6101–6106.
11. Sargent, E. H. Infrared Quantum Dots. *Adv. Mater.* **2005**, *17*, 515–522.
12. van Veggel, F. C. J M. Near-Infrared Quantum Dots and Their Delicate Synthesis, Challenging Characterization, and Exciting Potential Applications. *Chem. Mater.* **2014**, *26*, 111–122.
13. Doane, T. L.; Burda, C. The Unique Role of Nanoparticles in Nanomedecine: Imaging, Drug Delivery, and Therapy. *Chem. Soc. Rev.* **2012**, *41*, 2885–2911.
14. Yarema, M.; Pichler, S.; Sytnyk, M.; Seyrkammer, R.; Lechner, R. T.; Fritz-Popovski, G.; Jarzab, D.; Szendrei, K.; Resel, R.; Korovyanko, O.; *et al.* Infrared Emitting and Photoconducting Colloidal Silver Chalcogenide Nanocrystal Quantum Dots from a Silylamide-Promoted Synthesis. *ACS Nano* **2011**, *5*, 3758–3765.
15. Liu, Y.; Ko, D.; Oh, S. J.; Gordon, T. R.; Doan-Nguyen, V.; Paik, T.; Kang, Y.; Ye, X.; Jin, L.; Kagan, C. R.; *et al.* Near-Infrared Absorption of Monodisperse Silver Telluride (Ag_2Te) Nanocrystals and Photoconductive Response of Their Self-Assembled Superlattices. *Chem. Mater.* **2011**, *23*, 4657–4659.
16. Pons, T.; Pic, E.; Lequeux, N. Cassette, E.; Bezdetnaya, L.; Guillemin, F.; Marchal, F.; Dubertret, B. Cadmium-Free $CuInS_2$/ZnS Quantum Dots for Sentinel Lymph Node Imaging with Reduced Toxicity. *ACS Nano* **2010**, *4*, 2531–2538.
17. Zhong, H.; Wang, Z.; Bovero, E.; Lu, Z.; van Veggel, F. C. J. M.; Scholes, G. D. Colloidal $CuInSe_2$ Nanocrystals in the Quantum Confinement Regime: Synthesis, Optical Properties, and Electroluminescence. *J. Phys. Chem. C* **2011**, *115*, 12396–12402.
18. Kim, S.; Kang, M.; Kim, S.; Heo, J.-H.; Noh, J. H.; Im, S. H.; Seok, S. I.; Kim, S.-W. Fabrication of $CuInTe_2$ and $CuInTe_{2-x}Se_x$ Ternary Gradient Quantum Dots and Their Application to Solar Cells. *ACS Nano* **2013**, *7*, 4756–4763.
19. Hamanaka, Y.; Ogawa, T.; Tsuzuki, M. Photoluminescence Properties and Its Origin of $AgInS_2$ Quantum Dots with Chalcopyrite Structure. *J. Phys. Chem. C* **2011**, *115*, 1786–1792.
20. Chapman, G. H.; Shewchun, J.; Loferski, J. J.; Garside, B. K.; Beaulieu, R. Lattice Constants and Bandgap Variations of the System $Cu_{1-y}Ag_yInS_{(2-x)}Se_{2x}$. *Appl. Phys. Lett.* **1979**, *34*, 735–737.
21. Chang, J.-Y.; Wang, G. Q.; Cheng, C.-Y.; Lin, W.-X.; Hsu, J. C. Strategies for Photoluminescence Enhancement of $AgInS_2$ Quantum Dots and Their Application as Bioimaging Probes. *J. Mater. Chem.* **2012**, *22*, 10609–10618.
22. Mao, B.; Chuang, C.-H.; Lu, F.; Sang, L.; Zhu, J.; Burda, C. Study of the Partial Ag-to-Zn Cation Exchange in $AgInS_2$/ZnS Nanocrystals. *J. Phys. Chem. C* **2013**, *117*, 648–656.
23. Ng, M. T.; Boothroyd, C. B.; Vittal, J. J. One-Pot Synthesis of New-Phase $AgInSe_2$ Nanorods. *J. Am. Chem. Soc.* **2006**, *128*, 7118–7119.
24. Tian, L.; Ng, M. T.; Venkatram, N.; Ji, W.; Vittal, J. J. Tadpole-Shaped $AgInSe_2$ Nanocrystals from a Single Molecular Precursor and its Nonlinear Optical Properties. *Cryst. Growth Des.* **2010**, *10*, 1237–1242.
25. Wang, D.; Zheng, W.; Hao, C.; Peng, Q.; Li, Y. General Synthesis of I−III−VI_2 Ternary Semiconductor Nanocrystals. *Chem. Comm* **2008**, 2556–2558.
26. Abazović, N. D.; Čomor, M. I.; Mitrić, M. N.; Piscopiello, E.; Radetić, T.; Janković, I. A.; Nedeljović, J. M. Ligand Mediated

Synthesis of $AgInSe_2$ Nanoparticles With Tetragonal/Orthorhombic Crystal Phases. *J. Nanopart. Res.* **2012**, *14*, 810–820.
27. Allen, P. M.; Bawendi, M. G. Ternary I—III—VI Quantum Dots Luminescent in the Red to Near Infrared. *J. Am. Chem. Soc.* **2008**, *130*, 9240–9241.
28. Zhong, H.; Zhou, Y.; Ye, M.; He, Y.; Ye, J.; He, C.; Yang, C.; Li, Y. Controlled Synthesis and Optical Properties of Colloidal Ternary Chalcogenide CuInS2 Nanocrystals. *Chem. Mater.* **2008**, *20*, 6434–6443.
29. Saruyama, M.; Yeong-Gi, S.; Kimoto, K.; Taguchi, S.; Kanemitsu, Y.; Teranishi, T. Spontaneous Formation of Wurzite-CdS/Zinc Blende-CdTe Heterodimers through a Partial Anion Exchange Reaction. *J. Am. Chem. Soc.* **2011**, *133*, 17598–17601.
30. JCPDS. *Powder Diffraction File Alphabetical Index. Inorganic Phases*; JCPDS-International Centre for Diffraction Data: Swarthmore, PA, 1980.
31. Ogawa, T.; Kuzuya, T.; Hamanaka, Y.; Sumiyama, K. Synthesis of Ag—In Binary Sulfide Nanoparticles—Structural Tuning and Their Photoluminescence Properties. *J. Mater. Chem.* **2010**, *20*, 2226–2231.
32. Redjai, E.; Massé, G. Donor-Acceptor Pair Transitions in $AgInS_2$. *Phys. Status Solidi B* **1985**, *131*, K157–K159.
33. Massé, G.; Redjai, E. S-Vacancy Energy Levels in $AgInS_2$. *J. Appl. Phys.* **1986**, *59*, 1544–1547.
34. Krustok, J.; Raudoja, J.; Krunks, M.; Mandar, H.; Collan, H. Nature of the Native Deep Localized Defect Recombination Centers in the Chalcopyrite and Orthorhombic $AgInS_2$. *J. Appl. Phys.* **2000**, *88*, 205–209.
35. Li, L.; Daou, T. J.; Texier, I.; Chi, T. T. K.; Liem, N. Q.; Reiss, P. Highly Luminescent $CuInS_2$/ZnS Core/Shell Nanocrystals: Cadmium-Free Quantum Dots for *in Vivo* Imaging. *Chem. Mater.* **2009**, *21*, 2422–2429.
36. Landes, C.; Burda, C.; El-Sayed, M. A. Observation of Large Changes in the Band Gap Absorption Energy of Small CdSe Nanoparticles Induced by the Adsorption of a Strong Hole Acceptor. *Nano Lett.* **2001**, *1*, 667–670.
37. Uematsu, T.; Doi, T.; Torimoto, T.; Kuwabata, S. Preparation of Luminescent $AgInS_2$-$AgGaS_2$ Solid Solution Nanoparticles and Their Optical Properties. *J. Phys. Chem. Lett.* **2010**, *1*, 3283–3287.
38. Williams, A. T. R.; Winfield, S. A.; Miller, J. N. Relative Fluorescence Quantum Yields Using a Computer Controlled Luminescence Spectrometer. *Analyst* **1983**, *108*, 1067–1071.